Epigenetic regulation of DNA repair mediated by the histone methyltransferase DOT1L

Nehemiah S. Alvarez[1,2†]

[1]Department of Molecular and Integrative Physiology, University of Kansas Medical Center, Kansas City, Kansas, USA

[2]De Novo Genomics, Kansas City, KS, USA

[†]Corresponding author

Nehemiah S. Alvarez

3901 Rainbow Blvd

Kansas City, KS 66160

Email: nalvarez@kumc.edu

H2A.Z exchange at sites of DSB requires H3K79me

Keywords: HR, NHEJ, DNA repair, histone variants, epigenetic regulation

In eukaryotic cells, the homologous recombination (HR) and non-homologous end joining (NHEJ) pathways are required for the repair of DNA double strand breaks (DSB). In mammals, histone modification and histone variant exchange into nucleosomes at sites of DSB generate an open chromatin state necessary for repair to take place. How histone modifications contribute to histone variant exchange at DSB sites, and how this process results in DNA repair remain unresolved. Here we show that Disruptor of telomeric silencing -1 like (DOT1L) is required for H2A.Z histone variant exchange at DSB sites. Cells from Dot1L$^{-/-}$ mice have increased genomic instability and defects in DNA repair. Loss of either DOT1L or its methylation activity results in decreased H2A.Z incorporation at DSB sites, increased amounts of single strand DNA, and significantly reduced repair activity by homologous recombination.

Histone modifications and histone variant exchange are essential components of DNA repair pathways in eukaryotes. Phosphorylation of the histone variant H2A.X, termed γH2A.X, is an early histone modification that contributes to sensing DSB. The propagation of γH2A.X surrounding the break site leads to the recruitment

of the remodeling complex containing p400/Tip60 via the scaffolding protein MDC1 [1,2]. The p400-catalyzed exchange of H2A for H2A.Z into the nucleosome at DSB sites results in histone acetylation and histone ubiquitination [3]. These modifications serve as signals for the recruitment of several DSB repair factors, including BRCA1 and 53BP1, proteins necessary for both HR and NHEJ repair.

The extent to which histone-modifying enzymes participate in histone variant exchange at DSB sites is not well understood. The histone modifier DOT1L (Dot1 in yeast) is the only histone 3, lysine 79 (H3K79) methyltransferase in eukaryotic cells, and is responsible for deposition of mono, di and tri methyl marks [4,5]. A majority of Dot1L$^{-/-}$ mice die at mid-gestation, with defects in erythroid progenitor development, G1/G0 arrest, and increased apoptosis when treated with erythroid growth factors [6]. The anemic phenotype in Dot1L$^{-/-}$ mice is hypothesized to be due to loss of an erythroid-specific transcriptional program [6-11].

Accumulating evidence from eukaryotes indicates that Dot1/DOT1L is required for maintaining genome integrity, potentially by its involvement in the DNA damage response [12-16]. However, the precise role of Dot1L in the DNA damage response is unclear. Direct evidence for a role in DNA repair by DOT1L is limited, and the effects of DOT1L on genome stability have been attributed to alterations in the expression of DNA damage repair factors [17,18]. Also, Dot1L function in genome stability occurs in diverse cell types, suggesting that its function in DNA repair is not limited to a specific cell lineage. Based on the evidence of a role for Dot1L in genome stability, we hypothesize that the embryonic lethality of Dot1L$^{-/-}$ mice is due to a loss of DNA repair fidelity, resulting in the accumulation of unrepaired DNA lesions that halt embryogenesis.

Cells from Dot1L deficient mice have indicators of an unstable genome

Dot1L$^{-/-}$ mice have similar numbers of hematopoietic progenitors as wild-type littermates; however, cytokine-induced differentiation promotes their apoptosis[6]. To determine whether hematopoietic progenitors derived from Dot1L$^{-/-}$ mice accumulate DNA damage, cells from E10.5 yolk sacs were cultured in media containing cytokines that promote growth of erythroid and myeloid progenitors: SCF, IL-3, IL-6, and EPO. After 4 days of growth, cells were analyzed for endogenous DNA damage. In an alkaline comet assay, hematopoietic progenitors from Dot1L$^{-/-}$ mice showed significant increases in DNA damage when compared to progenitors derived from wild-type littermates (Fig. 1a).

Dot1L$^{-/-}$ embryos are smaller than wild-type littermates, suggesting that the absence of Dot1L might affect cell types other than hematopoietic progenitors [6]. To examine this, we assessed proliferation and accumulation of DNA damage in cells isolated from the embryo proper. Somatic cells isolated from E10.5 Dot1L$^{-/-}$ embryos had a delay in cell cycle progression, as demonstrated using an image analysis pipeline we termed MANA (machine autonomous nuclei analyzer) (Extended Data Fig. 1) [19]. The overall proportion of Dot1L$^{-/-}$ cells was greater in the G1/G0 phase, and lower in the G2/M phase compared to cells from wild-type controls (Fig. 1b). The G1/G0 accumulation recapitulated the results reported for Dot1L$^{-/-}$ yolk sac progenitors in erythroid differentiation cultures [6]. The Dot1L$^{-/-}$ cell proliferation defects were detrimental, because cell division slowed after three days in culture (Fig. 1c). We corroborated the proliferation defects using a microscopy-based BrdU incorporation assay, in which cells isolated from E10.5 embryos were pulsed for 24 hrs. Four days after isolation, there were fewer BrdU positive cells derived from Dot1L$^{-/-}$ embryos compared to cells from wild-type littermates (Extended Data Fig. 2). We also observed that cells isolated from Dot1L$^{-/-}$ embryos have an increased occurrence of micronuclei, a marker of genomic instability (Fig. 1d) [20,21]. These results indicate the presence of genome instability and defective proliferation, similar to the hematopoietic progenitors. It is conceivable that in the absence of Dot1L, these cells accumulate DNA damage that goes unrepaired. This would result in a highly unstable genome and slower cell cycle kinetics, which ultimately would lead to cell death.

An absence of Dot1L delays DNA repair and enhances RAD51 foci formation

We examined whether cells isolated from E10.5 embryos faithfully repair DNA following genotoxic stress. Low dose ionizing radiation (IR) was used to introduce DNA damage, and we assayed for DNA repair using an alkaline comet assay. Cells isolated from Dot1L$^{-/-}$ embryos and wild-type littermates have similar amounts of DNA damage at 24 hrs post IR (Fig. 2a). However, at 72 and 96 hrs post IR, cells from Dot1L$^{-/-}$ embryos have more accumulated DNA damage than wild-type cells (Fig. 2a). This indicates that after exposure to IR, E10.5 Dot1L$^{-/-}$ cells fail to completely repair DNA damage. The persistence of unrepaired DNA damage can lead to genome instability, cell cycle arrest, and apoptosis. Using a microscopy based BrdU incorporation assay, we observed that 96 hrs after IR treatment, both Dot1L$^{-/-}$ and wild-type cells continue to proliferate,

albeit at a slower rate (Extended Data Fig. 2, Extended Data Fig. 3a). This observation suggests that cells from E10.5 Dot1L$^{-/-}$ embryos continue to proliferate despite having DNA damage, which may account for the increased levels of endogenous DNA damage that we observe (Fig. 1a,d).

An accumulation of unrepaired DNA suggests that cells from Dot1L$^{-/-}$ embryos might have defects in DNA damage repair. Dot1L is hypothesized to be a transcriptional activator, so this increased DNA damage could be a result of decreased expression of DNA damage response (DDR) genes in the Dot1L$^{-/-}$ embryos [18,22]. We performed a gene expression analysis for DDR pathway factors in cells isolated from E10.5 embryos. Cells from Dot1L$^{-/-}$ embryos have elevated expression of several factors involved in sensing DNA damage, suggesting that some aspect of DDR transcription is intact (Extended Data Fig. 3b).

DNA damage is marked by γH2A.X, which is required for proper spatial and temporal recruitment of DDR factors. In Dot1L$^{-/-}$ cells exposed to 2 Gy of IR, γH2A.X DDR foci are elevated at all time points measured, compared to wild-type cells (Fig. 2b). This indicates that Dot1L$^{-/-}$ cells can detect DNA damage. However, the number of DNA damage sites continues to increase over time, suggesting that the DNA damage is not being repaired. This observation is consistent with the results of the comet assay (Fig 2a). Transcript expression analyses revealed that Dot1L$^{-/-}$ cells have elevated levels of Rad51 (Extended Data Fig. 3b). Increased abundance of RAD51 protein can drive genome instability by favoring the alternative NHEJ (alt-NHEJ) pathway [23]. We analyzed DDR foci formation of RAD51 in Dot1L$^{-/-}$ cells exposed to 2 Gy of IR and found that RAD51 foci were elevated compared to wild-type cells (Fig. 2c). We hypothesize that the enhanced RAD51 foci formation could favor alt-NHEJ usage in Dot1L$^{-/-}$ mice, and could account for the increase in genome instability we observed.

Loss of Dot1L methylation activity affects the timing of 53BP1 and BRCA1 accumulation in repair foci

The methyltransferase activity of Dot1L is purported to be involved in DNA repair [16,17]. However, in the Dot1L$^{-/-}$ mouse model, expression from the *Dot1L* locus is ablated using a gene trap [6]. This prevents an analysis of Dot1L function that distinguishes its role as a histone methyltransferase from any other potential function of the intact protein (e.g. its capacity to interact with other proteins). We utilized CRISPR/Cas9 to generate two DOT1L mutant HEK293T cell lines: *DOT1L*^{Stop} and *DOT1L*^{Y312A} (Extended Data Fig. 4) [24,25]. Both *DOT1L*^{Stop}

and *DOT1L*^{Y312A} HEK293T cells have decreased H3K79 di- and tri-methylation marks, while only *DOT1L*^{Stop} reduces DOT1L protein expression (Extended Data Fig. 4h).

After the formation of DSB, two criteria influence repair pathway utilization: the stage of the cell cycle in which the DSB occurs, and how quickly DNA damage repair factors assemble at DSB sites [26-29]. To gain insight into the mechanism by which DOT1L affects DDR factor loading, we examined the kinetics of 53BP1 and BRCA1 DNA damage foci formation, which occurs prior to RAD51 foci formation (Fig. 3a, b, & c, Extended Data Fig. 5). We treated wild-type, *DOT1L*^{Stop}, and *DOT1L*^{Y312A} cells with IR and analyzed 53BP1 foci formation at different time points (Extended Data Fig. 5a). We observed that at 30 and 60 minutes post IR, *DOT1L*^{Stop} and *DOT1L*^{Y312A} cells have reduced 53BP1 foci compared to wild-type HEK293T cells, but by 90 minutes, have similar numbers of foci per cell (Extended Data Fig. 5a). BRCA1 foci levels for *DOT1L*^{Stop} and wild-type cells are similar at all time points, however, *DOT1L*^{Y312A} cells have a significant decrease in foci abundance at 60 minutes post IR (Extended Data Fig. 5b).

53BP1 and BRCA1 coordinate and fine-tune the DDR at sites of double strand breaks [30,31]. Therefore, we compared the co-localization of 53BP1 and BRCA1 following IR treatment. We observed reduced 53BP1/BRCA1 co-localization events in both the *DOT1L*^{Stop} and *DOT1L*^{Y312A} mutant cells 30 minutes post IR (Fig. 3a). It has been reported that 53BP1 limits the end resection activity of BRCA1 during the S phase of the cell cycle [26,31]. We determined whether the ratios of 53BP1 to BRCA1 foci were differentially affected in *DOT1L*^{Stop} and *DOT1L*^{Y312A} cells following exposure to IR (Fig. 3b). At 30 minutes post IR, both *DOT1L*^{Stop} and *DOT1L*^{Y312A} cells display reduced ratios of 53BP1/BRCA1 during S phase (Fig. 3b). We also observed an increase in the population of BRCA1-positive S phase cells 30 minutes post IR in both mutant cell lines, but no compensatory increase in 53BP1-positive S phase cells (Fig. 3c, Extended Data Fig. 5d). We did not observe this phenomenon in the G1 populations of either cell line (Extended Data Fig. 5c, d). The decrease in co-localization of 53BP1/BRCA1 and increased amounts of BRCA1 positive S-phase cells indicate that the coordination between 53BP1 and BRCA1 in fine-tuning the DSB DDR is reduced.

Lack of H3K79 methylation reduces HDR activity

The altered BRCA1 and 53BP1 kinetics we observed in *DOT1L*^{Stop} and *DOT1L*^{Y312A} cells after exposure to IR led us to hypothesize that DDR repair pathway usage is affected. To test this hypothesis, we used three different reporter systems to monitor DDR pathway utilization: DR-GFP for HR, E5J-GFP for NHEJ, and E2J-GFP for alt-NHEJ [32,33]. We observed that both *DOT1L*^{Stop} and *DOT1L*^{Y312A} cell lines had substantial reductions in HR repair activity (Fig. 3d). *DOT1L*^{Stop} cells could still process breaks using NHEJ, but the *DOT1L*^{Y312A} cells had a slight reduction in NHEJ repair activity (Fig. 3e). We also examined the alt-NHEJ repair pathway, and *DOT1L*^{Stop} had a slight increase in repair activity compared to wild-type and *DOT1L*^{Y312A} cells (Fig. 3f). Suggesting that in the absence of DOT1L or its methylation activity, cells preferentially utilize error-prone DNA repair pathways to repair DSB.

H3K79 methylation is required for efficient H2A.Z incorporation into nucleosomes at sites of DSB

Recent work has indicated that histone exchange of H2A.Z into the nucleosomes surrounding DSB sites can influence DNA repair pathway utilization [3]. We hypothesized that H3K79 methylation might influence the stability of nucleosomes associated with DNA[34], so we examined the stability of H2A.Z containing nucleosomes association with DNA. Strikingly, we observed that H2A.Z is more stable in the *DOT1L*^{Stop} and *DOT1L*^{Y312A} cells following exposure to IR (Fig. 4a). Analyzing histone dynamics using stability assays have limited resolution, and information about local histone dynamics around specific DNA break sites is lost. Furthermore, the current methodology for assaying nucleosome dynamics at DSB sites relies on prior knowledge of the sequence composition surrounding the DSB, and overexpression of endonucleases whose time to expression is unknown. To address these limitations, we developed an assay that can monitor the histone dynamics at DSB with fine temporal resolution, independent of the underlying genomic sequence: BEL-ChIP (broken end ligation ChIP) (Extended Data Fig. 6a). We performed BEL-ChIP on H2A.Z and observed that *DOT1L*^{Stop} and *DOT1L*^{Y312A} cells have decreased enrichment of H2A.Z at DSB sites following exposure to IR (Fig. 4b). An interpretation of this result is that H2A.Z exchange in nucleosomes at DSB sites is defective in *DOT1L*^{Stop} and *DOT1L*^{Y312A} mutants.

We also examined the H4 acetylation state at DSB using BEL-ChIP. Evidence suggests that H4 acetylation can alter the relative ratios of BRCA1 and 53BP1 at DSB sites by preventing the association of

53BP1[28]. 53BP1 has been shown to be important for limiting end-resection activity in regions immediately adjacent to DSB sites [31]. We observe that global H4 acetylation is similar in wild-type, *DOT1L*^{Stop} and *DOT1L*^{Y312A} cells. Further, H4 acetylation occurs on the nucleosomes at the DSB sites, suggesting that the chromatin state is driven to a more open conformation, while lacking the boundary elements necessary to prevent hyper end resection (Extended data Fig. 6b & c).

H2A.Z nucleosome incorporation restricts the activity of the end resection machinery [3]. In the absence of H2A.Z, end resection is thought to be over-active, and favors the generation of single stranded DNA (ssDNA) [3]. In yeast, Dot1 mutants have increased amounts of end resection, but this has not been reported in a mammals [12,35]. We designed an assay to measure the length of ssDNA using Oxford Nanopore technology. We observe that following exposure to IR, *DOT1L*^{Stop} and *DOT1L*^{Y312A} mutants generate longer ssDNA than wild-type cells (Fig. 4c, Extended Data Fig. 6d). Since ssDNA is a poor substrate for HR, this result is consistent with the observation that both *DOT1L*^{Stop} and *DOT1L*^{Y312A} cells have defective HR repair activity [3].

Discussion

Recent findings demonstrate that histone variant exchange around sites of DSB can influence DNA repair pathway utilization by limiting end resection activity [36]. These results expand upon this idea by demonstrating that DOT1L and DOT1L-histone methylation can influence H2A.Z exchange into nucleosomes at DSB sites and are consistent with earlier suggestions that altered 53BP1 and BRCA1 kinetics lead to increased ssDNA and the utilization of mutagenic DNA repair pathways [26,31]. The data suggest a model in which DOT1L methylation activity facilitates the efficient incorporation of H2A.Z into nucleosomes at sites of DSB (Fig. 4d). The lack of H2A.Z at these sites allows enhanced end resection activity, and promotes the generation of long ssDNA, which decreases the efficiency of HDR [3].

The role of Dot1L in transcriptional activation suggests the accumulation of lesions observed in the Dot1L$^{-/-}$ mice could be a consequence of a down regulated DNA damage-specific transcriptional program. However, contrary to this view, we observed significant increases in transcripts required for DSB repair, indicating that cells from Dot1L$^{-/-}$ mice are transcriptionally primed for DSB repair. Despite this, Dot1L$^{-/-}$ cells accumulate DNA lesions and fail to repair induced DNA damage, indicating that the defect in repair is post-

transcriptional. Dot1L$^{-/-}$ mice have enhanced RAD51 foci formation, suggesting that in the absence of H3K79 methylation, cells might preferentially utilize the highly mutagenic alt-NHEJ repair pathway [23]. Further dissection of DOT1L function using CRISPR/Cas9 generated mutants (*DOT1L*^{Stop} and *DOT1L*^{Y312A}) demonstrate that the kinetics of 53BP1 and BRCA1 repair foci formation are altered. BRCA1 and 53BP1 are recruited to DSB prior to RAD51 and define the region surrounding the DSB. Alterations of these factors have been shown to result in the utilization of highly mutagenic DNA repair pathways [3,31]. Consistent with this observation, the absence of DOT1L or H3K79 methylation, cells have a substantial reduction in the utilization of HDR pathways, while maintaining the mutagenic pathway of alt-NHEJ.

DSB repair pathway utilization can be modulated by H2A.Z incorporation into nucleosomes surrounding the break site [3]. We postulated that alterations in the DNA damage foci kinetics observed in DOT1L mutant cells were a result of changes in H2A.Z nucleosome incorporation. This, in part, was motivated by the observation that H3K79 methylation alters nucleosome surface properties [34]. In the absence of H3K79 methylation, H2A.Z displayed increased stability. We reasoned that if H2A.Z containing nucleosomes could not be removed efficiently from the genome following DSB, then there could be a defect in H2A.Z incorporation into nucleosomes at sites of DSB. Currently methodologies for assaying histone dynamics at DSB sites lack the temporal and spatial resolution needed to measure these changes on a genome-wide scale. We therefore developed BEL-ChIP, and assayed H2A.Z dynamics in DOT1L mutant cells. We found that H2A.Z containing nucleosomes immediately adjacent to DSB sites are substantially reduced. Alterations in H2A.Z nucleosome incorporation in DOT1L mutants could be a product of alterations in nucleosome composition. It has been observed that H3.1 and H2A.Z containing nucleosomes are as stable as H3.1/H2A containing nucleosomes [37]. In the absence of H3K79 methylation, there could be a decrease in the H3.3/H2A.Z nucleosomes and an increase in H3.1/H2A.Z nucleosomes, which could result in reduced dissociation from the genome. Evidence suggests that H3K79 methylation occurs predominantly on H3.3, so it would be interesting to determine whether H3.3/H2A.Z nucleosome assembly requires H3K79 methylation [38].

A consequence of disrupted H2A.Z nucleosome incorporation following the formation of DSB is an increase in end resection [3]. Overactive end resection would favor the generation of longer strands of ssDNA.

Consistent with this model, we found that induction of DSB in the absence of either DOT1L or H3K79 methylation resulted in the production of significantly longer ssDNA. Long ssDNA is a poor substrate for HDR and can favor the utilization of mutagenic repair pathways [3,31]. The increased ssDNA substrate observed in *DOT1L*^{Stop} and *DOT1L*^{Y312A} mutant cell lines could also be an explanation for the increase in RAD51 DDR foci we observe in cells isolated from Dot1L$^{-/-}$ mice (Fig 2c). RAD51 binds to ssDNA, forming filaments necessary for HDR to take place [39]. However, as the length of ssDNA increases, more mutagenic repair pathways are used [23,31]. These results provide novel insight into the function of DOT1L in DNA repair and provide a mechanism for the observation that DOT1L-deficient cells have unstable genomes.

The correlation of H3K79 methylation with active transcription has been used to support the hypothesis that DOT1L is a transcriptional activator [22]. Similarly, the enrichment of H2A.Z at the promoters of actively transcribed genes caused it to be defined as a factor necessary for transcriptional activation [40]. We propose an alternative interpretation for these observations. In the case of H3K79 methylation and H2A.Z, we propose that these factors mark regions of the genome that require HDR. This interpretation of the data would entail that the transcriptional program of a cell would be primed for HDR. Interestingly, rearrangements in MLL genomes, which results in the relocalization of DOT1L, do not disrupt the efficiencies of NHEJ, HDR, and alt-NHEJ [41]. We propose that relocalization of DOT1L in MLL leukemia protects the leukemic transcriptional program from DNA damage. Curiously, ChIP experiments with H2A.Z indicate that sites of endonuclease-induced DSB are reminiscent of promoters [3]. It may be that transcriptional activation and DNA repair are more closely linked than is currently appreciated. We predict that as the temporal resolution of DNA repair factor assembly improves, more factors associated with active transcription will be revealed as factors associated with DNA repair.

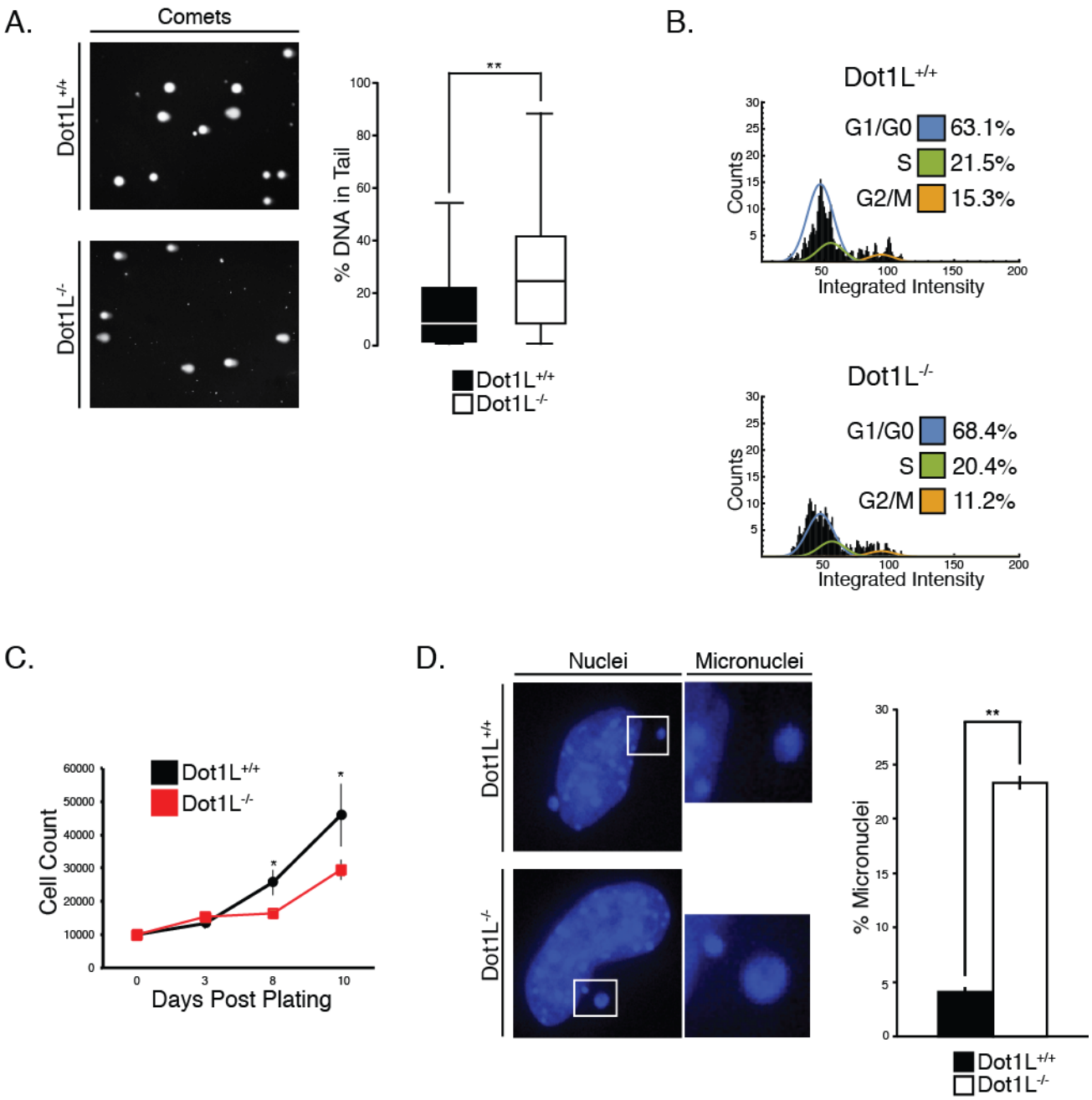

Figure 1 | Dot1L$^{-/-}$ mouse embryonic cells display genomic instability. a. Distribution of DNA tail content from a comet assay of *ex vivo* differentiated erythroid cells isolated from E10.5 yolk sacs. b. Cell cycle distribution of cells isolated from the embryo proper of E10.5 mice. c. Growth kinetics of cells isolated from the embryo proper of E10.5 mice. Data are mean ±sem, n=3. d. Percentage of cell isolated from the embryo proper of E10.5 mice that contain micronuclei. Data are mean ±sem, n=3. *$P < 0.05$, **$P < 0.01$.

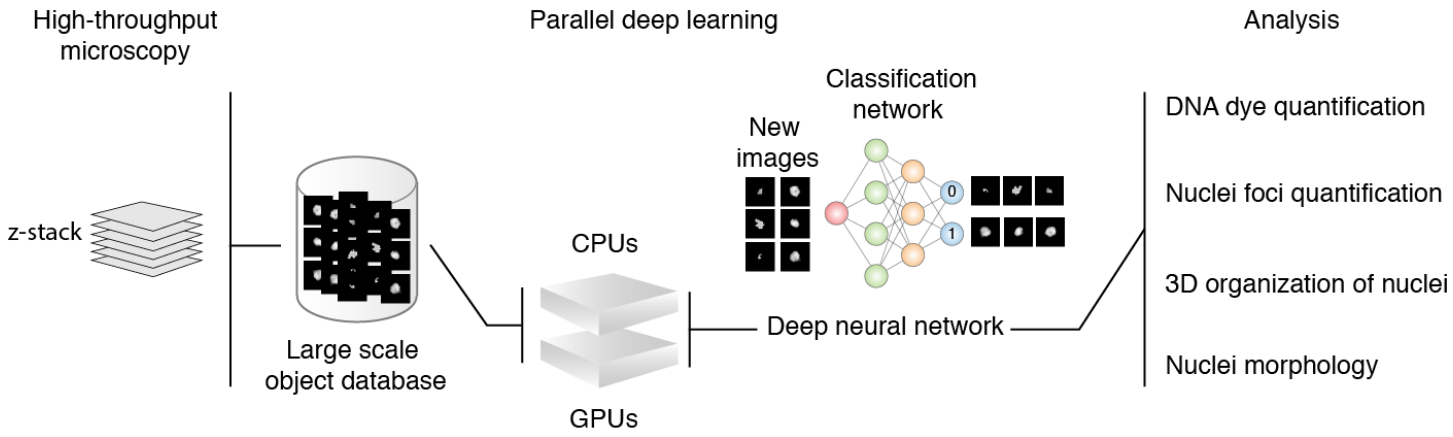

Extended Data Figure 1 | MANA (machine autonomous nuclei analyzer) pipeline overview. High-resolution microscopy images are segmented to isolate objects. The segmented objects are classified into two groups; nuclei and non nuclei, by a deep learning neural network. Subsequent steps quantify foci amount and cycle stage by calculating the intensity profiles of nuclei in 2D and 3D space.

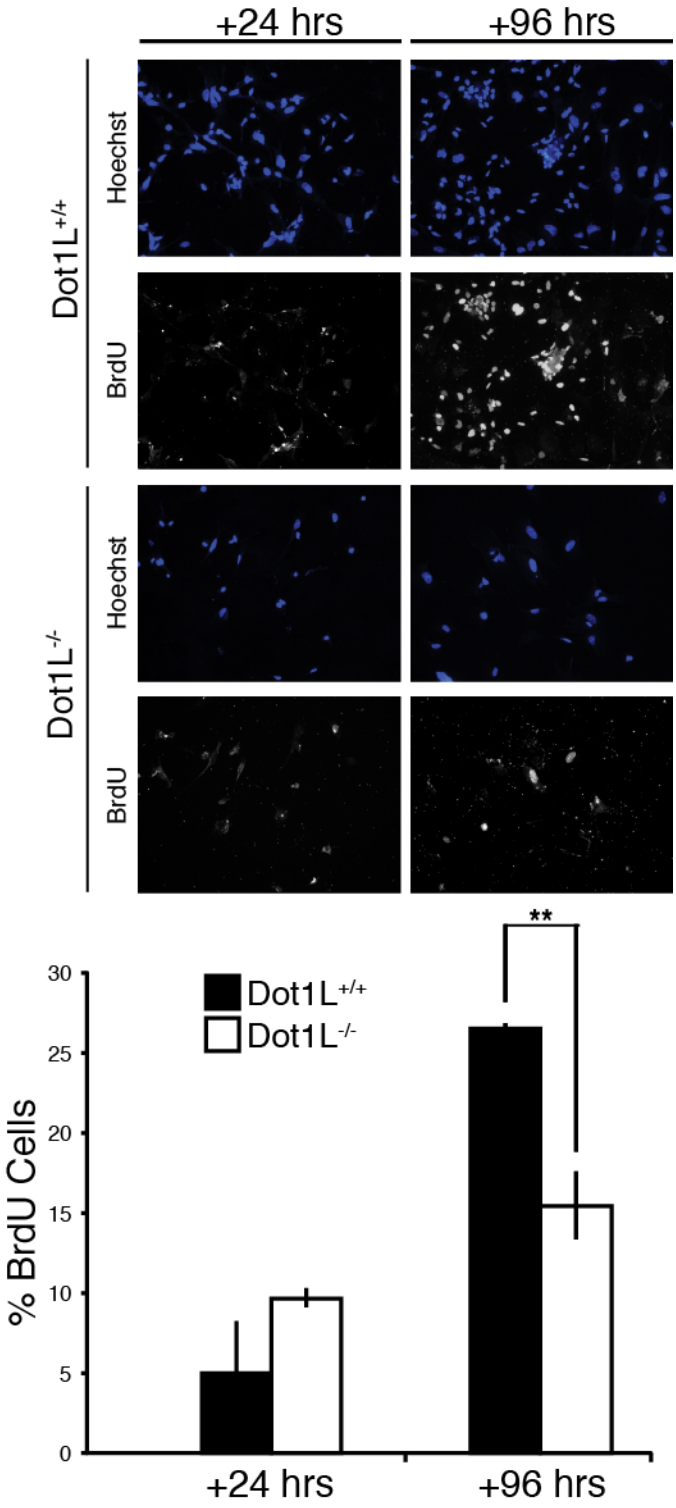

Extended Data Figure 2 | Dot1L$^{-/-}$ mouse embryonic cells have reduced proliferative capacity. BrdU assay of cells isolated from the embryo proper of E10.5 mice. Data are mean ±sem, n=3. *$P < 0.05$, **$P < 0.01$.

A.

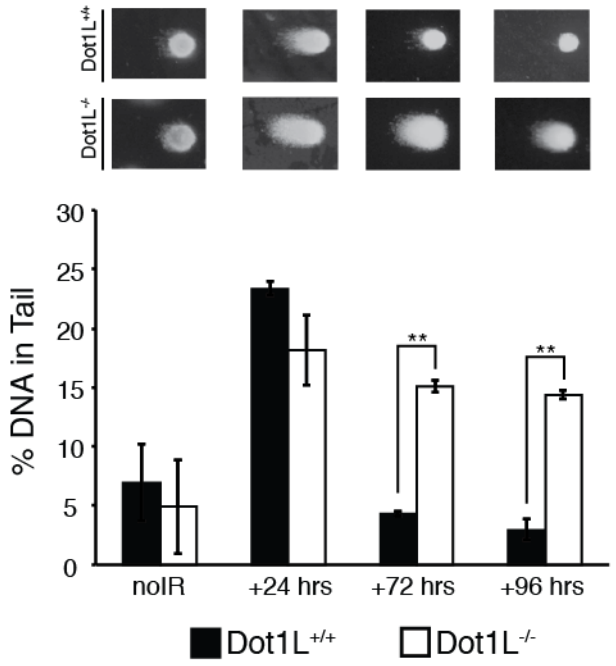
Dot1L+/+
Dot1L-/-
% DNA in Tail
30
25
20
15
10
5
0
**
**
noIR
+24 hrs
+72 hrs
+96 hrs
Dot1L+/+
Dot1L-/-

B.

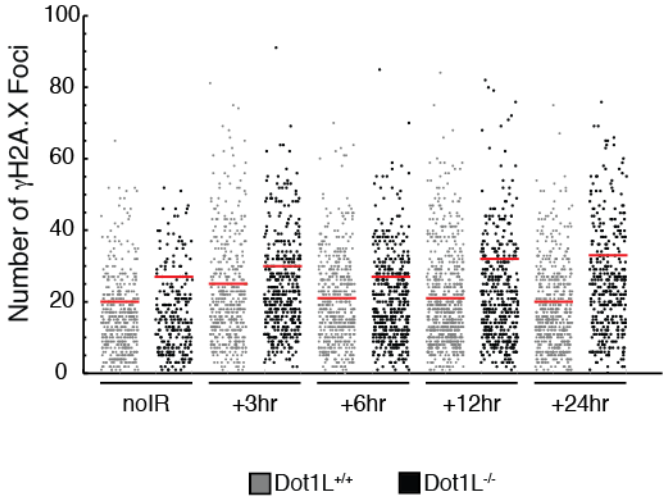
Number of γH2A.X Foci
100
80
60
40
20
0
noIR
+3hr
+6hr
+12hr
+24hr
Dot1L+/+
Dot1L-/-

C.

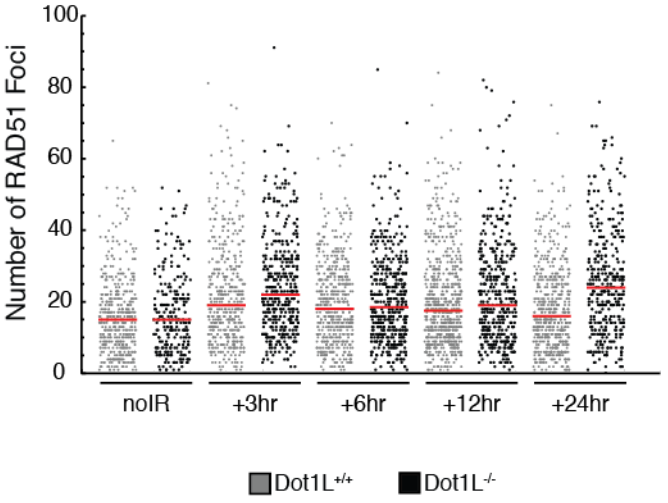
Number of RAD51 Foci
100
80
60
40
20
0
noIR
+3hr
+6hr
+12hr
+24hr
Dot1L+/+
Dot1L-/-

Figure 2 | Dot1L$^{-/-}$ mouse embryonic cells have reduced DNA damage repair capacity. a. Mean of % DNA tail content from a comet assay of E10.5 embryonic cells exposed to 2 Gy of IR. Data are mean ±sem, n=3. b, – c. Distribution of γH2A.X, and RAD51 foci in E10.5 embryonic cells at 3, 6, 12, and 24 hrs post exposer to 2 Gy of IR, noIR (no IR exposure), median (orange). *$P < 0.05$, **$P < 0.01$.

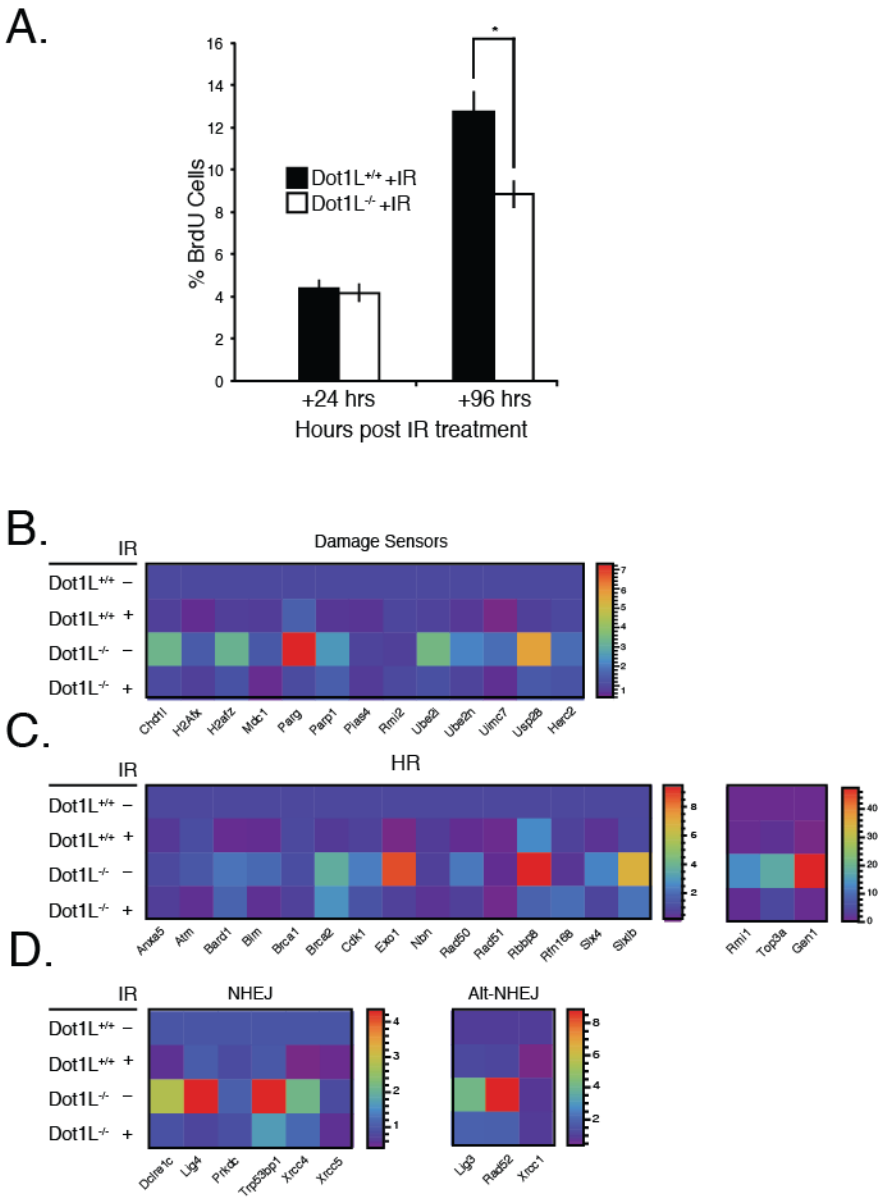

Extended Data Figure 3 | Dot1L$^{-/-}$ mouse embryonic cells have elevated expression of DNA damage response factors. a. Mean % of BrdU positive cells from E10.5 embryonic cells exposed to 2 Gy of IR. Data are mean ±sem, n=3. b.–d. Expression of DNA damage sensors (b), HR factors (c), and NHEJ factors (d) from E10.5 embryonic cells exposed to 2 Gy of IR. Scale indicates the ΔCt value. *$P < 0.05$, **$P < 0.01$.

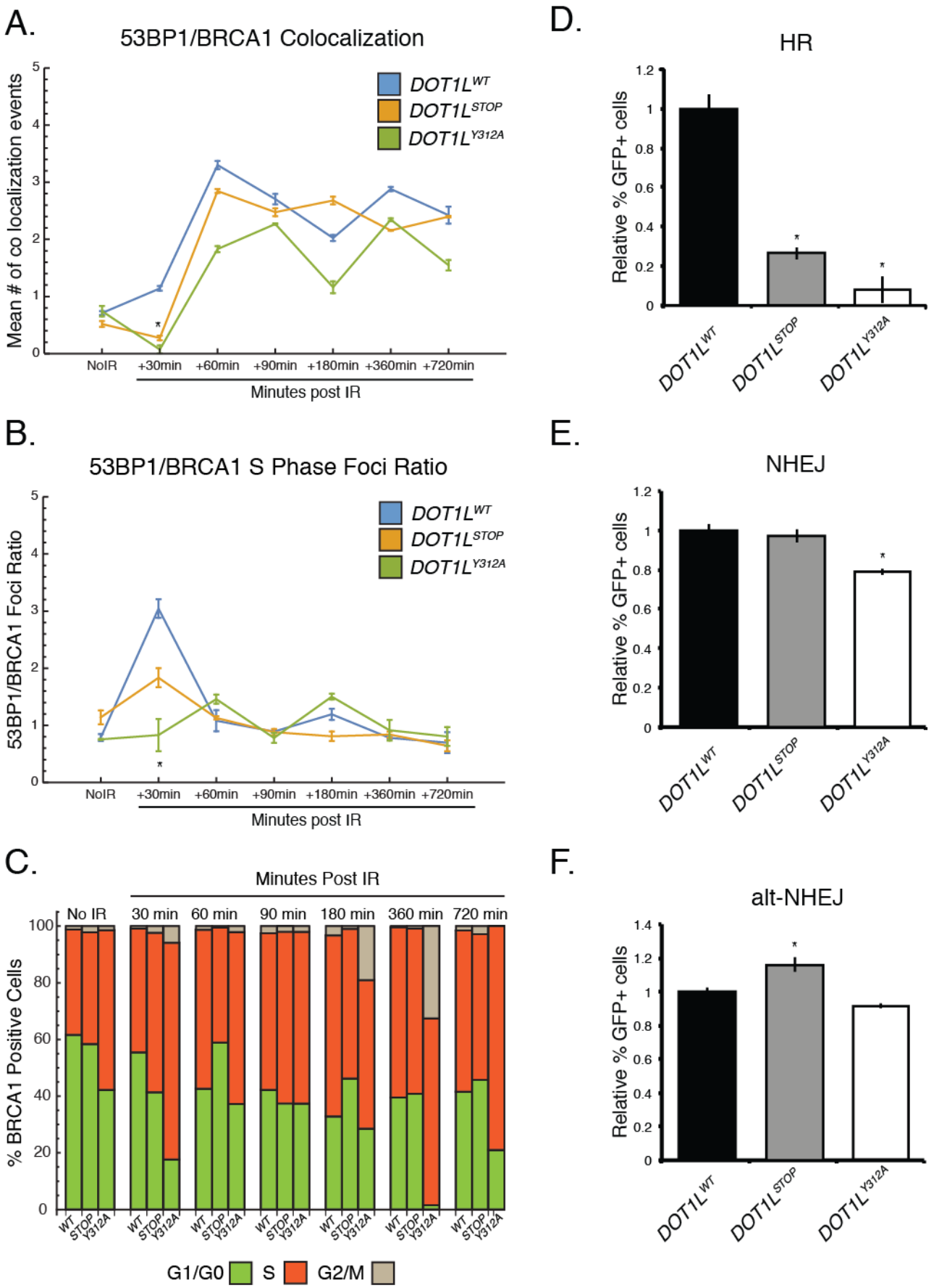
A.
53BP1/BRCA1 Colocalization
Mean # of co localization events
DOT1L^WT
DOT1L^STOP
DOT1L^Y312A
NoIR
+30min
+60min
+90min
+180min
+360min
+720min
Minutes post IR
B.
53BP1/BRCA1 S Phase Foci Ratio
53BP1/BRCA1 Foci Ratio
C.
Minutes Post IR
No IR
30 min
60 min
90 min
180 min
360 min
720 min
% BRCA1 Positive Cells
WT
STOP
Y312A
G1/G0
S
G2/M
D.
HR
Relative % GFP+ cells
E.
NHEJ
F.
alt-NHEJ

Figure 3 | *DOT1L*^{STOP} and *DOT1L*^{Y312A} mutant cells have altered 53BP1/BRCA1 foci kinetics and defects in DNA damage repair pathway usage. a. Mean of 53BP1/BRCA1 co-localized foci in cells exposed to 10 Gy of IR. Data are mean ±sem, n=3. *P<0.05 wild-type vs. *DOT1L*^{STOP}, wild-type vs. *DOT1L*^{Y312A}. b. Mean of the ratio of 53BP1/BRCA1 foci in cells exposed to 10 Gy of IR in the S phase of cell cycle. Data are mean ±sem, n=3. *P<0.05 wild-type vs. *DOT1L*^{STOP}, wild-type vs. *DOT1L*^{Y312A}. c. Percentage of BRCA1 positive cells in each phase of the cell cycle following exposure to 10 Gy of IR. d. Stable cell lines expressing the DR-GFP reporter transfected with the I-Sce1 endonuclease. Data are mean ±sem, n=3. e. Stable cell lines expressing the E5J-GFP reporter transfected with the I-Sce1 endonuclease. Data are mean ±sem, n=3. f. Stable cell lines expressing the E2J-GFP reporter transfected with the I-Sce1 endonuclease. Data are mean ±sem, n=3. *$P < 0.05$, **$P < 0.01$.

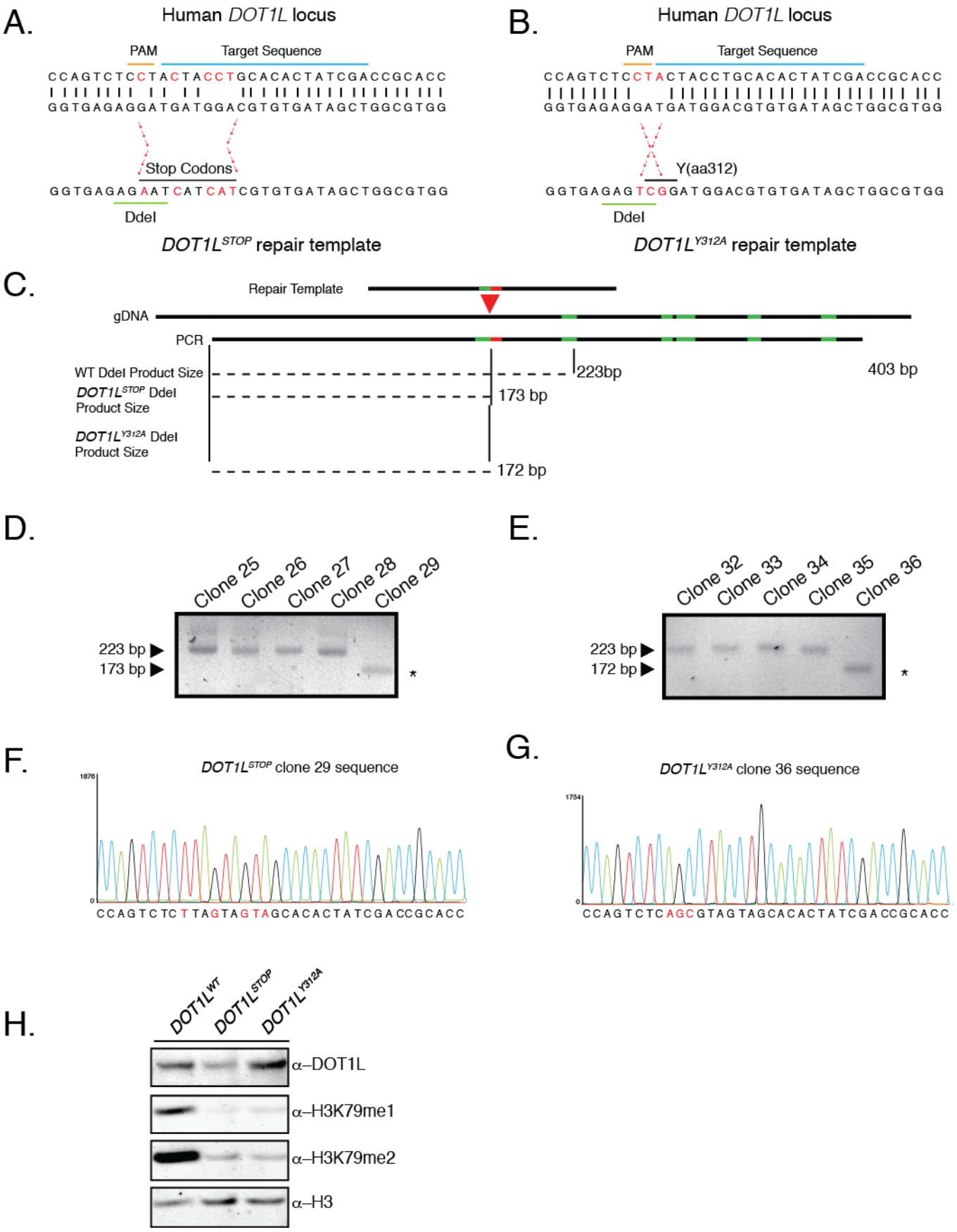
A.
Human DOT1L locus
PAM
Target Sequence
CCAGTCTCCTACTACCTGCACACTATCGACCGCACC
GGTGAGAGGATGATGGACGTGTGATAGCTGGCGTGG
Stop Codons
GGTGAGAGAATCATCATCGTGTGATAGCTGGCGTGG
DdeI
DOT1L^STOP repair template
B.
Human DOT1L locus
PAM
Target Sequence
CCAGTCTCCTACTACCTGCACACTATCGACCGCACC
GGTGAGAGGATGATGGACGTGTGATAGCTGGCGTGG
Y(aa312)
GGTGAGAGTCGGATGGACGTGTGATAGCTGGCGTGG
DdeI
DOT1L^Y312A repair template
C.
Repair Template
gDNA
PCR
WT DdeI Product Size
223bp
403 bp
DOT1L^STOP DdeI Product Size
173 bp
DOT1L^Y312A DdeI Product Size
172 bp
D.
Clone 25
Clone 26
Clone 27
Clone 28
Clone 29
223 bp
173 bp
*
E.
Clone 32
Clone 33
Clone 34
Clone 35
Clone 36
223 bp
172 bp
*
F.
DOT1L^STOP clone 29 sequence
CCAGTCTCTTAGTAGTAGCACACTATCGACCGCACC
G.
DOT1L^Y312A clone 36 sequence
CCAGTCTCAGCGTAGTAGCACACTATCGACCGCACC
H.
DOT1L^WT
DOT1L^STOP
DOT1L^Y312A
α–DOT1L
α–H3K79me1
α–H3K79me2
α–H3

Extended Data Figure 4 | Generation of *DOT1L*^{STOP} and *DOT1L*^{Y312A} mutant cells using CRISPR/Cas9. a. & b. Sub-region of Human *DOT1L* locus with the CRISPR/Cas9 spacer sequence (blue) and PAM (orange). Nucleotides targeted for mutation are labeled in red, the region of interest in the single stranded oligonucleotide repair template is below, the added DdeI site is underlined in green. c. PCR and DdeI resection digest screening strategy. d. & e. Subset of clones screened using PCR and DdeI digest to identify insertion. Positive clones are marked with asterisk. f. & g. Representative Sanger sequence of clones positive for mutation. h. Example western blot of a positive clone.

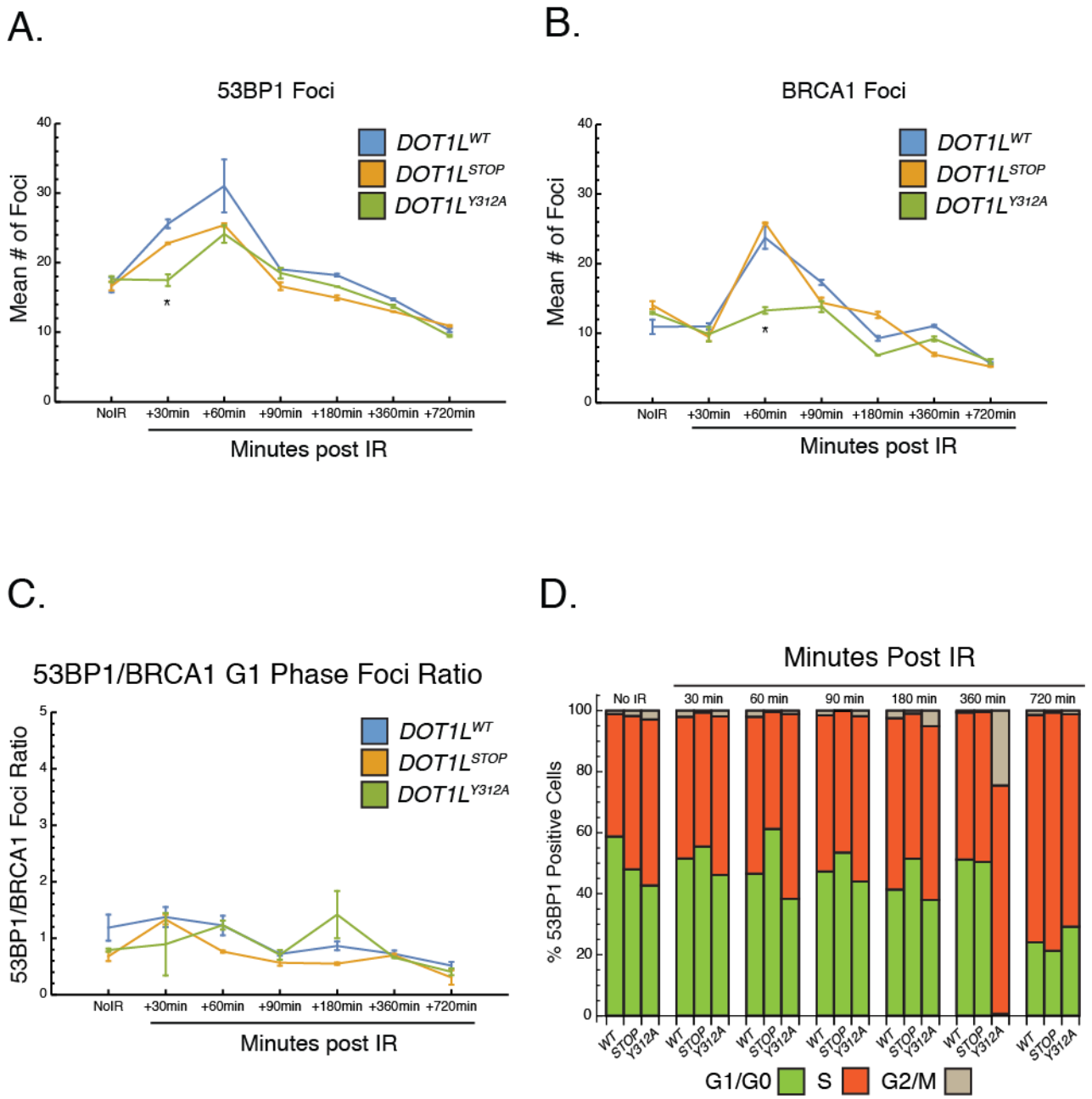

Extended Data Figure 5 | *DOT1L*^{STOP} and *DOT1L*^{Y312A} mutant cells have reduced 53BP1 and BRCA1 foci formation, but normal G1 53BP1/BRCA1 foci ratio and normal 53BP1 cell cycle distribution. a. Mean of 53BP1 foci in cells exposed to 10 Gy of IR. Data are mean ±sem, n=3. *P<0.05 wild-type vs. *DOT1L*^{Y312A}. b. Mean of the ratio of BRCA1 foci in cells exposed to 10 Gy of IR. Data are mean ±sem, n=3. *P<0.05 wild-type vs. *DOT1L*^{Y312A}. c. Mean of the ratio of 53BP1/BRCA1 foci in cells exposed to 10 Gy of IR in the G1 phase of cell cycle. Data are mean ±sem, n=3. d. Percentage of 53BP1 positive cells in each phase of the cell cycle following exposure to 10 Gy of IR. *$P < 0.05$, **$P < 0.01$.

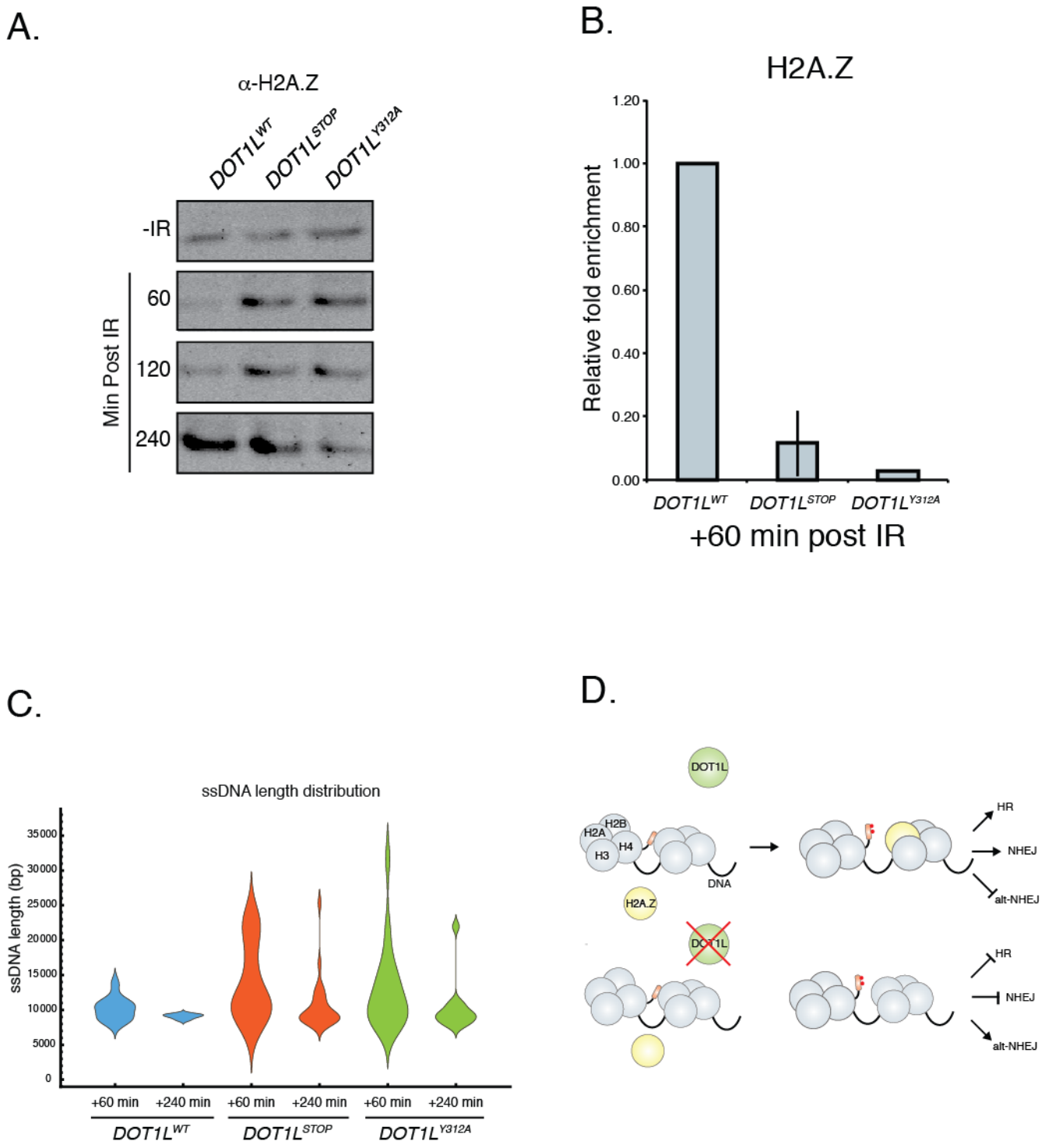

Figure 4 | *DOT1L^STOP* and *DOT1L^Y312A* mutant cells have defects in H2A.Z incorporation at sites of double strand breaks. a. Histone stability assay following exposure to 10 Gy of IR. Western H2A.Z. b. BEL-ChIP of H2A.Z at sites of double strand breaks. Data are mean ±sem, n=3. c. Length distribution of ssDNA after exposure to 10 Gy IR. Normalized to No IR input for each sample d. Model for the role of DOT1L in DSB repair.

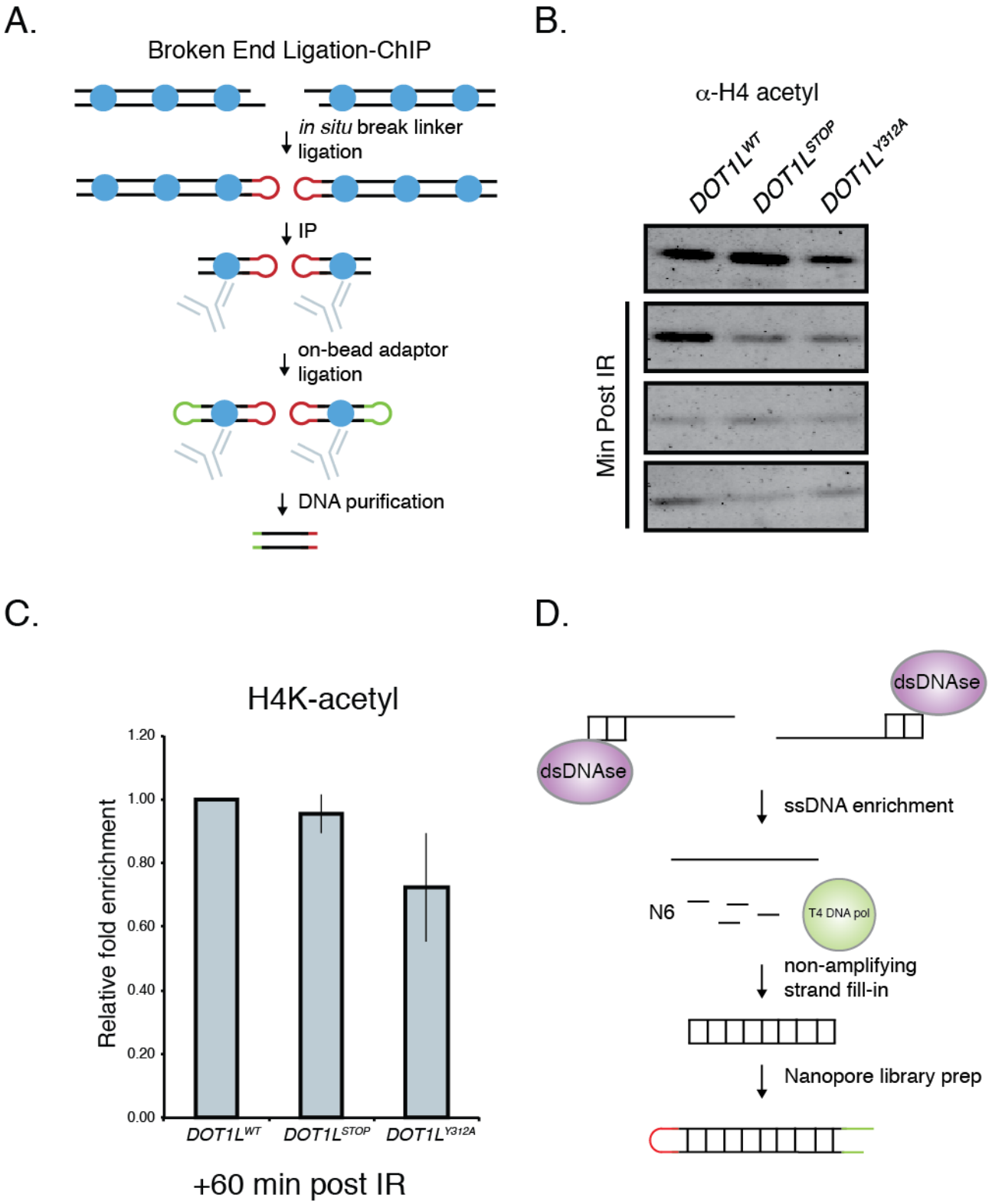

Extended Data Figure 6 | *DOT1L*^{STOP} and *DOT1L*^{Y312A} mutant cells have normal H4 acetylation levels at double strand break sites. a. Diagram of BEL-ChIP assay. b. Histone stability assay following exposure to 10 Gy of IR. Western H4 acetylation. c. BEL-ChIP of H2A.Z at sites of double strand breaks. Data are mean ±sem, n=3. d. Diagram of ssDNA enrichment for sequencing on Oxford Nanopore MinION.

Methods

Dot1L knockout mice. Dot1L$^{-/-}$ mice were generated as described [6].

***Ex vivo* erythroid differentiation assay**. Cells from E10.5 *Dot1L*$^{-/-}$ and wild-type yolk sacs cultured in M3434 methylcellulose medium (StemCell Technologies) containing the cytokines SCF, IL-3, IL-6, and EPO, which promote the growth of erythroid and myeloid progenitors.

Cell Culture. Wild type HEK293T and mutant HEK293T *DOT1L*^{STOP} and *DOT1L*^{Y312A} cell lines were maintained in 10% FBS, DMEM, Pen/Strep in 37 ^{o}C, 5% CO_2. Embryonic day 10.5 (E10.5) embryos were obtained from timed matings between heterozygous Dot1L mutant mice, cells were isolated from the whole embryo and cultured in DMEM, high glucose, L-glutamate, Sodium Pyruvate (Life Technologies, 11995-040), 10% fetal bovine serum (Life Technologies 10082-147), supplemented with 20 mM HEPES (Life Technologies 15630-080), L-glutamte, and Non-essential amino acids.

Cas9 Targeting of HEK293T cells. *DOT1L*^{Stop} and *DOT1L*^{Y312A} cell lines were generated by Cas9/ssDNA directed cleavage/repair. The CRISPR/Cas9 vector pX330-U6-Chimeric_BB-CBh-hSpCas9 was a gift from Feng Zhang (Addgene plasmid # 42230)[42]. The CRISPR/Cas9 vector was modified to express an eGFP-P2A-Cas9 fusion gene using SLiCE (Seamless Ligation Cloning Extract) method [43]. Briefly, overlapping PCR was used to generate eGFP-P2A cDNA with arms of homology for pX330 promoter and N-terminus of hSpCas9. 2 µL of SLiCE was mixed with eGFP-P2A cDNA and digested pX330 in a 1:4 molar ratio and incubated at 37°C for 1 hr. 2 µL of the reaction was transformed into *e. coli*. Single clones were isolated and verified by Sanger sequencing. SLiCE strain of *e.coli* was a gift from Yongwei Zhang. The guide RNA targeting the *DOT1L* locus was cloned into eGFP-P2A-Cas9 using BbsI. The same guide RNA was used to generate both *DOT1L*^{Stop} and *DOT1L*^{Y312A} cell lines. DOT1L amino acid 312 was chosen for targeting because previous in vitro demonstrated that mutation to this residue H3K79 methylation activity was disrupted and it satisfied CRISPR/Cas9 targeting parameters [44,45].150 nt single stranded oligonucleotide, antisense to transcription, was used to direct repair of the Cas9 cleaved locus by destroying the PAM, adding a DdeI restriction site and either adding three tandem stop codons (*DOT1L*^{Stop}) or nucleotides converting Tyrosine 312 to Alanine (*DOT1L*^{Y312A}). HEK293T (ATCC) cells were transfected with a 1:1 molar ratio of eGFP-P2A-Cas9 and single stranded oligonucleotide using Effectine

(Qaigen) in a six well dish. Cells were sorted for eGFP expression 48 hrs after transfection (FACSaria II, BD). Colonies were picked 5 days later, genomic DNA was extracted and a PCR/restriction digest with DdeI was used to initially identify DOT1L and Y312A positive clones. Western blot and Sanger sequencing was used to verify clones.

The following primers were used to PCR screen for mutations:

DOT1L Screen Forward: GTG TGG GAG AAG AGG GAA GA

DOT1L Screen Reverse: AGC AGT ACT GAG GGG CCT TG

The following primers were used for cloning the guide RNA into the CRIPSR/Cas9 vector:

DOT1L Guide Forward: CAC CGT CGA TAG TGT GCA GGT AGT

DOT1L Guide Reverase: AAA CAC TAC CTG CAC ACT ATC GAC

The following sequences are the repair templates used to generate the *DOT1L* mutants:

DOT1L Stop Repair Template:

CAG GAC GGC CCT GCG GCT GAG GCG CAG CGA GAT ACT CAC TAT GGT GCG GTC GAT AGT GTG CTA CTA CTA AGA GAC TGG CTT CCC CGT CCA CGA CAC TGA TCC TTT CAG GGG CGA GAG CTC CAC CAC GCG CAT GAT GGT GCC GAT GTC TGC

DOT1L Y312A Repair Template:

CAG GAC GGC CCT GCG GCT GAG GCG CAG CGA GAT ACT CAC TAT GGT GCG GTC GAT AGT GTG CAG GTA GGC TGA GAC TGG CTT CCC CGT CCA CGA CAC TGA GCC CTT CAG GGG CGA GAG CTC CAC CAC GCG CAT GAT GGT GCC GAT GTC TGC

Immunofluorescence. HEK293T *DOT1L*^{STOP} and *DOT1L*^{Y312A} cell lines and cells isolated from E10.5 Dot1L$^{-/-}$ and wild-type embryos were plated onto cover slips treated with L-Poly lysine (75 000 -150 000 MW). Cells were exposed to 10 Gy of ionizing radiation. Cells were fixed at different time points post irradiation with 4% Paraformaldhyde for 30 min at room temperature, cells were washed with 200mM Glycine/1X DPBS for 10 min, permeablized with 0.2 % TritonX100/1X DPBS for 30min, blocked with 1% BSA/1XDPBS for 60 min. Mouse DDR foci were visualized by staining with gH2A.X (Abcam #ab2893,1:1000), RAD51(Abcam #ab133534, 1:1000), 53BP1(Abcam #ab36823, 1:500) for 1 hr, followed by secondary antibody AlexFlour 488

(ThermoFisher # A-11008, 1:1000) for 2 hrs. HEK293T cells were co-stained with 53BP1(Abcam #ab36823, 1:500) and BRCA1 (Abcam #ab16781, 1:2000) was visualized by staining for 1 hr, followed by secondary antibody AlexFlour 488 (ThermoFisher # A-11008, 1:1000) and AlexFlour 594 (ThermoFisher # A-11001, 1:2500) for 2 hrs. Cells were washed with 1X DPBS/Hoechst (1µg/mL) 3 times for 5 minutes.

Western antibodies .H3K79 di meth (Abcam #ab3594), H3K79 mono meth (Abcam #ab2886), H3 (Abcam #ab24834), Dot1L (Abcam #ab57827), H2A.Z (CellSignaling #2718,).

DNA damage pathway gene expression. Total RNA was isolated from cells of E10.5 *Dot1L*$^{-/-}$ and wild-type mice that were 6 hours post ionizing radiation treatment (2 Gy). qPCR was performed using Power SYBR® Green PCR Master Mix (#4367659, Thermofisher Scientific), primers with annealing temperature of 61°C and 40 cycles on ABI 7900 system. Primers for mouse DNA damage pathway genes were designed using IDT PrimerQuest Tool.

Gene	**Fwd**	Rev
Anxa5	CGAATAGAGACCCTGATACTGC	ACTGCGTGTCCCAAAGATG
Atm	GATCCTTCCCACTCCAGAAAC	ACTCCGCATAACTTCCATCG
Bard1	TCCCGCTGTGCTAATATTCTG	GTCGGTTTATCTTGAGGTCTAGG
Blm	TGGATCAGAAAGCATCACCC	GTAAAGTGTCAGCCATTGTGTC
Brca1	AGGGAAGCACAAGGTTTAGTC	CCTCATTCAAACGCTCACAAG
Brca2	CTTTAGAGCCGGTTACCTGTG	AGGACTGCTTGGAGACTTTTC
Cdk1	TGCAGGACTACAAGAACACC	GCCATTTTGCCAGAGATTCG
Dclre1c	TCGTGTGGCTGAACTGTAAAG	TTCTGTCCGTTGTGAGATGG
Exo1	CAGTAGGGATTCAGGTTCAGAG	ACTAGACCTACAGAGCCCAG
Gen1	TGCCGTTGATTTGAGTCTCTG	TCCCCTTCCATTACAAACACC
H2afx	AAGTCGCGCTCTTCACG	TCTCGGCAGTGAGGTACTC
H2afz	GTATCACCCCTCGTCACTTG	TCTTCTGTTGTCCTTTCTTCCC
Herc2	ACACCAGGCATACTTTCGG	GTTCAGGCTTTTCACCATTCG
Lig3	AGTGGGAATGAAGAGGAAAGC	GTGTAGAAGGTGGCAAGTAGAG
Lig4	CCCCTGTGATTGCTGACTTAG	TCTCGTGGCTTCAATTCTGG
Mdc1	TGATTGACTGGGATGCTGAAG	CATTCTTGCCAAGGTAGAGGG
Nbn	CCTTTCCCAAGTCCTGTCAG	CAGCCCAGGGATCTTTACTTC
Parg	GATTGTTTCACGGCTGTTCAC	ATCGTCCTTTTCACTCCCATC
Parp1	CAGCGAGAGTATTCCCAAGG	AAGCCATCCACCTCAACATC
Pias4	CCTTACCCACCTCATGTATCTG	TCACCCCAATCGTCTTCAAC
Prkdc	TTCTCCATACCCAAACCCAAG	CTCCCAGTCAGCCAATCAAA
Rad50	AGTGTGCCTGACAGATGTTAC	GCTTTTCCTGCTTTTCCTGG
Rad51	TGGTGTCGCAGTGGTAATC	CTCCCCTCTTCCTTTTCTCAG
Rad52	CCAGCATGTTCTAGGTAGCAG	TCCTTTTGTGACGGTCTAGTG
Rbbp8	CCAAGCAACCAAGATACGTCC	TCCATGTCCACTGTTTCTCC

Rmi1	GATCCTACAGTTCCAGTCATTCC	GCCCCAAAACAGCATCTAAG
Rnf168	TGAACGACTTGCTGGAGAAC	TTCGACAAATGGGACACTCTAC
Slx1b	GGAAGAGGATTTGGAGTTAGAGG	GAGAAGCAGGAAAGGTACAGG
Slx4	CTGAACTACCTCTACATGGCAG	TCTGGCTGTTCTCCCTCTAAG
Top3a	GTCTTGTCCTTTATCAGTTGTGC	CAATTTCCGAGATGCCAGTTTC
Trp53bp1	CCCTGATGCTTTCCGATCTAC	TCTGTCTCCATTGCTTCGTC
Ube2i	GAACCAAATATTCAAGACCCAGC	CAATCCCTTCCTCGTCATGG
Ube2n	TGATGTAGCCGAGCAATGG	TTGGCAGAACAGGAGAAGTG
Uimc1	TGATGGAGCAGGAAACAGTG	GTGGAACCAGGGACTTACATAG
Usp28	GTGACATTACCACTTCCCTCG	CATTCATCCCCTCAGAGCTG
Xrcc1	GCTGGGACCGTGTTAAAATTG	GTCACTGTCACCTTCTGAGATG
Xrcc4	TGGGACAGAACCTAAAATGGC	GGGTAGTGAAGAGGCAAGC
Xrcc5	TGACTGCTCAGGACGTTTTC	CCTTGGTGATGTTCCCTTCTG

ssDNA measurement and MinION sequencing. Wild type HEK293T and mutant HEK293T *DOT1L*^{STOP} and *DOT1L*^{Y312A} cell lines were exposed to 10 Gy of ionizing radiation and total genomic DNA was isolated at 60 and 240 min post radiation exposure. Genomic DNA was isolated by adding resuspending cell pellets in 50 µL of Extraction buffer (Tris-HCl, pH 9.5, 0.1M, KCl 0.25 M, EDTA 0.01 M), 10 µL Proteinase K (20 mg/mL), 10 µL RNAseA (10 mg/mL, Fermentas). The samples were incubated at 55°C for 15 minutes and ethanol precipitated. The extracted DNA was digested with RNAse A and dsDNAse (ThermoFisher) overnight at room temperature. The samples were ethanol precipitated and twice. ssDNA was converted to dsDNA using the following reaction 5 µL dNTP, 2µL AMP Ligase (ThermoFisher), 2µL T4 DNA polymerase, 10µL Random hexamer, 5 µL Ligase buffer. Reaction was incubated at 25°C for 10 min and 16 ^{o}C for 16 hrs. The samples were precipitated and the sequencing library was prepared as described in MinION documentation. Base calling was performed by Metrichor 2.42.2 and sequence analysis was performed using the Mathematic programming language. DNA molecules present in the NoIR samples were subtracted from the +60 min and +240 min post IR samples.

BEL-ChIP. The Broken end linker and Anchor linker (IDT) were annealed using T4 DNA Ligase Reaction Buffer (#B0202S, New England Biolabs) to a final concentration of 10µM. The reaction was heated to 98°C for 5 minutes and allowed to cool to room temperature at 1°C per minute. Wild type HEK293T and mutant HEK293T *DOT1L*^{STOP} and *DOT1L*^{Y312A} cell lines were plated into 10 cm dishes two days prior to treatment of

ionizing radiation. On the day of experiment, cells were trypsinized, neutralized with 500 µL 10% FBS, 1X DMEM, and centrifuged at 300xg for 7 minutes to pellet. Cells were treated with 10 Gy ionizing radiation following manufactures recommendations. Cells were gently resuspended and placed in a 37 ^{o}C, 5% CO_2 incubator for 60 minutes. 54 µL 37% Formaldehyde (2% Final conc.) was added to the sample, and incubated with constant rotation at room temperature for 30 minutes. 62.5 µL of 2 M Glycine (125 mM) was added to the samples and incubated with constant rotation at room temperature for 5 min. Cells were pelleted at 300xg for 7 minutes at 4 ^{o}C and then washed three times with ice cold PBS (-Ca^{2+},Mg^{2+}). Cells were resuspended in 1mL of ice cold Buffer A + 0.5 µL 1M DTT + 5 µL 200X PIC (SimpleChIP Kit #9003, Cell Signaling Technology) and incubated on ice 10 minutes with mixing every 3 minutes. Cells were harvested at 3000 rpm for 5 minutes at 4 ^{o}C. The pellet was washed 3X with 500 µL NEBuffer 2.1 (#B7202S, New England Biolabs). The pellet was resuspended in 88 µL of NEBuffer 2.1, 10 µL dNTP (1mM, #N0446S, New England Biolabs), 2 µL T4 DNA Polymerase (#M0203S,New England Biolabs). The reaction was incubated at RT for 45 minutes with gentle mixing every 5 minutes. The sample was then washed 3X with 500 µL ice cold T4 DNA Ligase Reaction + 0.1% Triton X100 (#T8787, Sigma Aldrich). The pellet is then washed once with 500 µL T4 DNA Ligase Reaction Buffer. The pellet was resuspended in 18.5 µL T4 DNA Ligase Reaction Buffer with 5 µL of 10µM annealed Broken end linker and 1.5 µL T4 DNA Ligase (#M0202S, New England Biolabs). The reaction was incubated 18-20 hours at 16 ^{o}C with constant mixing. The samples were washed 3X with T4 DNA Ligase Reaction + 0.1% Triton X100. The pellets were resuspended in 100 µL ChIP Buffer (SimpleChIP Kit #9003, Cell Signaling Technology), 2 µL RNAse A (10mg/mL, # EN0531, Thermo Fisher Scientific) and sonicated 30 seconds on and 30 seconds off for 45 minutes at 4°C. Samples were centrifuged at 10,000 rpm for 10 minutes at 4 ^{o}C, transferred to new tubes and frozen at -80 ^{o}C. ChIP was performed using an amount of BEL-ChIP nuclear extract corresponding to 3.4 µg of input genomic DNA in 250 µL of ChIP Buffer + 1X PIC (SimpleChIP Kit #9003, Cell Signaling Technology). Antibody was added to manufacture specifications and incubated overnight with end over end mixing at 4 ^{o}C. 30 µL magnetic protein G beads (SimpleChIP Kit #9003, Cell Signaling Technology) were added to the samples and incubated at 4 ^{o}C with end over end rotation for 4 hours. A magnetic rack was used to collect the beads and the sample was washed 2X with 500 µL NEBuffer 2.1. The

beads were resuspended in 100 µL of NEBuffer 2.1, 10 µL 1mM dNTP, 2 µL T4 DNA Polymerase and incubated at room temperature for 25 minutes with constant shaking. The beads were placed in a magnetic rack to clear the supernatant and washed 2X with 500 µL ice cold T4 DNA Ligase Reaction Buffer. The beads were resuspended 50 µL T4 DNA Ligase Reaction Buffer with 5µL of 10µM annealed Anchor linker and 1.5 µL T4 DNA Ligase. The sample was incubated overnight at room temperature with constant shaking. The beads were washed and DNA was purified following the SimpleChIP Kit procedure. Purified DNA from the ChiP procedure (25 µL) was digested with 1 uL of I-SceI endonuclease (#R0694S, New England Biolabs) for 1 hour and heat inactivated. PCR of 10 cycles and annealing temperature 61°C was performed using Q5 High-Fidelity DNA Polymerase (#M0491S, New England Biolabs) and BEL and AL primers on 5µL of I-SceI digested DNA purified from the ChIP procedure. PCR reactions were run on a 2% agarose gel (NuSieve™ GTG™, Lonza) and the 200-400 bp region was excised and purified using a QIAquick Gel Extraction Kit (#28704, Qiagen). qPCR was performed using Power SYBR® Green PCR Master Mix (#4367659, Thermofisher Scientific), BEL and AL primers with annealing temperature of 61 ^{o}C and 40 cycles on ABI 7900 system.

Broken End Linker

TACTACCTCGAGTAGGGATAACAGGGTAATTTTTTATTACCCTGTTTATCCCTACTCGAGGTAGTA

Anchor Linker

CGTCGTCTCGAGTAGGGATAACAGGGTAATTTTTTATTACCCTGTTTATCCCTACTCGAGACGACG

BEL Primer

TTATCCCTATCTCGAGGTAGTA

AL Primer

TTATCCCTACTCGAGACGACG

Cell cycle staging and foci analysis. Cell cycle staging and foci quantification were performed on cells isolated from E10.5 *Dot1L*$^{-/-}$, wild-type mice, HEK293T wild-type, *DOT1L*^{Stop} and *DOT1L*^{Y312A} cell lines using MANA (Machine autonomous nuclei analyzer). Briefly, MANA was coded for in Mathematica and utilizes convolutional (deep learning) neural network for nuclei classification. The neural network was trained using human curated nuclei images and the data set was expanded to 180,000 nuclei images from both primary and

tissue culture cells. Cell cycle staging was performed by using Watson method for cell cycle peak calling [46]. Microscopy images were collected on a Nikon TE2000 Inverted microscope with a 40X objective, 0.6 NA.

HR/NHEJ assays. Wild-type, *DOT1L*^{Stop} and *DOT1L*^{Y312A} HEK293T cell lines expressing an HR reporter [33], alt-NHEJ reporter [32], and a NHEJ reporter [32], were transfected individually with Effectine (Qiagen) and selected for using puromycin. Five days post-transfection, cells were transfected with the I-SceI plasmid using Effectine, and GFP-positive cells were counted 48 hr later using a Invitrogen Attune. GFP values were normalized to the wild-type sample.

Nucleosome stability assay. The nucleosome stability is described in [36]. Wild-type, *DOT1L*^{Stop} and *DOT1L*^{Y312A} cell lines were exposed to 10 Gy ionizing radiation and harvested at 30, 60, and 240 minutes post IR. Cells were washed with ice-cold PBS and resuspended in 500 µL of Stability buffer (20 mM Hepes, pH 7.9, 0.5 mM DTT, 1.5 mM MgCl 2, 0.1% Triton) containing 1.0 M NaCl, Roche Protease Inhibitor cocktail) and agitated constantly for 40 min at 4 °C. Cells were collected by centrifugation at 100,000 × g (Beckmann Ultracentrifuge) for 20 min, and the supernatant was removed and the genomic DNA was resuspended in 100 µL ChIP Buffer (SimpleChIP Kit #9003, Cell Signaling Technology), 2 µL RNAse A (10mg/mL, # EN0531, Thermo Fisher Scientific) and sonicated 30 seconds on and 30 seconds off for 45 minutes at 4°C. The DNA content was analyzed and all samples were adjusted to have 3.4µg/mL concentration of DNA. A 1:10 dilution was made and 10µL were analyzed by western.

Comet assay and analysis. The alkaline comet assay for Fig. 1a was performed using the Trevigen Comet Assay kit (Trevigen, Gaithersburg, MD). Cells were isolated from yolk sacs of E10.5 *Dot1L*$^{-/-}$ and wild-type mice grown *ex vivo* differentiation media (see above), after 4 days cells were harvested and resuspended in cold PBS, and an aliquot of cells (1000/10 µl) was added to 100 µl of molten LMA agarose and spread onto a comet slide. The manufactures protocol for alkaline comet assay was followed without modification. The slides were imaged using an upright Nikon Eclipse 80i fluorescence microscope at ×20, and analyzed using CometScore Pro (TriTek Corp). A neutralizing comet assay was used for monitoring the repair of induced DNA damage, Fig. 2a. Cells were isolated from E10.5 *Dot1L*$^{-/-}$ and wild-type mice and exposed to 2 Gy of ionizing radiation

and a neutralizing comet assay was performed as specified in the manufactures protocol. Comets were analyzed using a custom comet analysis software development in Mathematic programing language.

Statistical analysis. Sample sizes for each experiment are as follows: Fig. 1a: 100 > cells from 3 wild-type mice, > 100 cells from 3 Dot1L$^{-/-}$ mice. Fig. 1b: n > 1000 cells wild-type mice, n > 1000 cells Dot1L$^{-/-}$ mice. Fig. 1c: n = 3 wild-type mice, n =3 Dot1L$^{-/-}$ mice. Fig. 1d: n > 1000 cells wild-type mice, n > 1000 cells Dot1L$^{-/-}$ mice. Extended Data Fig. 2 & Extended Data Fig. 3a: n = 3 wild-type mice, n =3 Dot1L$^{-/-}$ mice. Fig. 2a: n = 3 wild-type mice, n =3 Dot1L$^{-/-}$ mice. Fig. 2b, 2c: n=3, >1000 cells each wild-type mice, n = 3, >1000 cells each Dot1L$^{-/-}$ mice. Fig. 3a, 3b, Extended Data Fig. 5a, 5b, 5c: n=3, >250 cells each wild-type HEK293T cells, n=3, > 250 cells each *DOT1L*^{STOP} and *DOT1L*^{Y312A} cells. Fig. 3c & Extended Data Fig. 5d: n > 1000 cell wild-type HEK293T cells, n > 1000 cells each *DOT1L*^{STOP} and *DOT1L*^{Y312A} cells. Fig. 3d, 3e, 3f: n=3, HEK293T cells, n=3 *DOT1L*^{STOP} and *DOT1L*^{Y312A}. Analysis was carried out in comparison to the control group. Two-sided t-tests were used for control vs. mutant: Fig. 1c, Fig. 1d, Extended Data Fig. 2, Fig. 2a, Extended Data Fig. 3a, Fig. 3d, Fig. 3e, Fig. 3f. Mann-Whitney test was used for control vs. mutant: Fig. 1a, Fig. 2b, Fig. 2c, Fig. 3d. Two way ANOVA Tukey's multiple comparison test was used for multiple comparison of groups: Fig. 3a, Fig. 3b, Extended Data Fig. 5a, Extended Data Fig. 5b, Extended Data Fig. 5c. All experiments were repeated three times unless indicated.

Code availability. Code used for MANA and comet analysis is available upon request.

Acknowledgements. I would like to thank Drs. Patrick Fields, Fariba Behbod, Timothy Fields, Kenneth Peterson, Joseph Fontes, Pavla Brachova for their valuable feed back and guidance.

REFERENCES

1 Xu, Y. *et al.* The p400 ATPase regulates nucleosome stability and chromatin ubiquitination during DNA repair. *The Journal of cell biology* **191**, 31-43, doi:10.1083/jcb.201001160 (2010).

2 Downs, J. A. *et al.* Binding of chromatin-modifying activities to phosphorylated histone H2A at DNA damage sites. *Mol Cell* **16**, 979-990, doi:10.1016/j.molcel.2004.12.003 (2004).

3 Xu, Y. *et al.* Histone H2A.Z controls a critical chromatin remodeling step required for DNA double-strand break repair. *Mol Cell* **48**, 723-733, doi:10.1016/j.molcel.2012.09.026 (2012).

4 Feng, Q. *et al.* Methylation of H3-Lysine 79 Is Mediated by a New Family of HMTases without a SET Domain. *Current Biology* **12**, 1052-1058, doi:10.1016/s0960-9822(02)00901-6 (2002).

5 Ng, H. H. *et al.* Lysine methylation within the globular domain of histone H3 by Dot1 is important for telomeric silencing and Sir protein association. *Genes & development* **16**, 1518-1527, doi:10.1101/gad.1001502 (2002).

6 Feng, Y. *et al.* Early mammalian erythropoiesis requires the Dot1L methyltransferase. *Blood* **116**, 4483-4491, doi:10.1182/blood-2010-03-276501 (2010).

7 Lowenberg, B. Acute myeloid leukemia: the challenge of capturing disease variety. *Hematology Am Soc Hematol Educ Program*, 1-11, doi:10.1182/asheducation-2008.1.1 (2008).

8 Meyer, C. *et al.* New insights to the MLL recombinome of acute leukemias. *Leukemia* **23**, 1490-1499, doi:10.1038/leu.2009.33 (2009).

9 Mueller, D. *et al.* A role for the MLL fusion partner ENL in transcriptional elongation and chromatin modification. *Blood* **110**, 4445-4454, doi:10.1182/blood-2007-05-090514 (2007).

10 Okada, Y. *et al.* hDOT1L links histone methylation to leukemogenesis. *Cell* **121**, 167-178, doi:10.1016/j.cell.2005.02.020 (2005).

11 Steger, D. J. *et al.* DOT1L/KMT4 recruitment and H3K79 methylation are ubiquitously coupled with gene transcription in mammalian cells. *Molecular and cellular biology* **28**, 2825-2839, doi:10.1128/MCB.02076-07 (2008).

12 Lazzaro, F. *et al.* Histone methyltransferase Dot1 and Rad9 inhibit single-stranded DNA accumulation at DSBs and uncapped telomeres. *The EMBO journal* **27**, 1502-1512, doi:10.1038/emboj.2008.81 (2008).

13 Wysocki, R. *et al.* Role of Dot1-dependent histone H3 methylation in G1 and S phase DNA damage checkpoint functions of Rad9. *Molecular and cellular biology* **25**, 8430-8443, doi:10.1128/MCB.25.19.8430-8443.2005 (2005).

14 Giannattasio, M., Lazzaro, F., Plevani, P. & Muzi-Falconi, M. The DNA damage checkpoint response requires histone H2B ubiquitination by Rad6-Bre1 and H3 methylation by Dot1. *The Journal of biological chemistry* **280**, 9879-9886, doi:10.1074/jbc.M414453200 (2005).

15 Botuyan, M. V. *et al.* Structural basis for the methylation state-specific recognition of histone H4-K20 by 53BP1 and Crb2 in DNA repair. *Cell* **127**, 1361-1373, doi:10.1016/j.cell.2006.10.043 (2006).

16 Wakeman, T. P., Wang, Q., Feng, J. & Wang, X. F. Bat3 facilitates H3K79 dimethylation by DOT1L and promotes DNA damage-induced 53BP1 foci at G1/G2 cell-cycle phases. *The EMBO journal* **31**, 2169-2181, doi:10.1038/emboj.2012.50 (2012).

17 Huyen, Y. *et al.* Methylated lysine 79 of histone H3 targets 53BP1 to DNA double-strand breaks. *Nature* **432**, 406-411, doi:10.1038/nature03114 (2004).

18 FitzGerald, J. *et al.* Regulation of the DNA damage response and gene expression by the Dot1L histone methyltransferase and the 53Bp1 tumour suppressor. *PloS one* **6**, e14714, doi:10.1371/journal.pone.0014714 (2011).

19 Roukos, V., Pegoraro, G., Voss, T. C. & Misteli, T. Cell cycle staging of individual cells by fluorescence microscopy. *Nature protocols* **10**, 334-348, doi:10.1038/nprot.2015.016 (2015).

20 Crasta, K. *et al.* DNA breaks and chromosome pulverization from errors in mitosis. *Nature* **482**, 53-58, doi:10.1038/nature10802 (2012).

21 Zhang, C. Z. *et al.* Chromothripsis from DNA damage in micronuclei. *Nature* **522**, 179-184, doi:10.1038/nature14493 (2015).
22 Mohan, M. *et al.* Linking H3K79 trimethylation to Wnt signaling through a novel Dot1-containing complex (DotCom). *Genes & development* **24**, 574-589, doi:10.1101/gad.1898410 (2010).
23 Richardson, C., Stark, J. M., Ommundsen, M. & Jasin, M. Rad51 overexpression promotes alternative double-strand break repair pathways and genome instability. *Oncogene* **23**, 546-553, doi:10.1038/sj.onc.1207098 (2004).
24 Mali, P. *et al.* RNA-guided human genome engineering via Cas9. *Science* **339**, 823-826, doi:10.1126/science.1232033 (2013).
25 Jinek, M. *et al.* A programmable dual-RNA-guided DNA endonuclease in adaptive bacterial immunity. *Science* **337**, 816-821, doi:10.1126/science.1225829 (2012).
26 Chapman, J. R. *et al.* RIF1 is essential for 53BP1-dependent nonhomologous end joining and suppression of DNA double-strand break resection. *Mol Cell* **49**, 858-871, doi:10.1016/j.molcel.2013.01.002 (2013).
27 Luo, K., Zhang, H., Wang, L., Yuan, J. & Lou, Z. Sumoylation of MDC1 is important for proper DNA damage response. *The EMBO journal* **31**, 3008-3019, doi:10.1038/emboj.2012.158 (2012).
28 Tang, J. *et al.* Acetylation limits 53BP1 association with damaged chromatin to promote homologous recombination. *Nature structural & molecular biology* **20**, 317-325, doi:10.1038/nsmb.2499 (2013).
29 Watanabe, S. *et al.* JMJD1C demethylates MDC1 to regulate the RNF8 and BRCA1-mediated chromatin response to DNA breaks. *Nature structural & molecular biology* **20**, 1425-1433, doi:10.1038/nsmb.2702 (2013).
30 Panier, S. & Boulton, S. J. Double-strand break repair: 53BP1 comes into focus. *Nature reviews. Molecular cell biology* **15**, 7-18, doi:10.1038/nrm3719 (2014).
31 Ochs, F. *et al.* 53BP1 fosters fidelity of homology-directed DNA repair. *Nature structural & molecular biology* **23**, 714-721, doi:10.1038/nsmb.3251 (2016).
32 Bennardo, N., Cheng, A., Huang, N. & Stark, J. M. Alternative-NHEJ is a mechanistically distinct pathway of mammalian chromosome break repair. *PLoS genetics* **4**, e1000110, doi:10.1371/journal.pgen.1000110 (2008).
33 Pierce, A. J., Johnson, R. D., Thompson, L. H. & Jasin, M. XRCC3 promotes homology-directed repair of DNA damage in mammalian cells. *Genes & development* **13**, 2633-2638 (1999).
34 Lu, X. *et al.* The effect of H3K79 dimethylation and H4K20 trimethylation on nucleosome and chromatin structure. *Nature structural & molecular biology* **15**, 1122-1124, doi:10.1038/nsmb.1489 (2008).
35 Chen, X. *et al.* The Fun30 nucleosome remodeller promotes resection of DNA double-strand break ends. *Nature* **489**, 576-580, doi:10.1038/nature11355 (2012).
36 Gursoy-Yuzugullu, O., Ayrapetov, M. K. & Price, B. D. Histone chaperone Anp32e removes H2A.Z from DNA double-strand breaks and promotes nucleosome reorganization and DNA repair. *Proceedings of the National Academy of Sciences of the United States of America* **112**, 7507-7512, doi:10.1073/pnas.1504868112 (2015).
37 Jin, C. & Felsenfeld, G. Nucleosome stability mediated by histone variants H3.3 and H2A.Z. *Genes & development* **21**, 1519-1529, doi:10.1101/gad.1547707 (2007).
38 McKittrick, E., Gafken, P. R., Ahmad, K. & Henikoff, S. Histone H3.3 is enriched in covalent modifications associated with active chromatin. *Proceedings of the National Academy of Sciences of the United States of America* **101**, 1525-1530, doi:10.1073/pnas.0308092100 (2004).
39 Liu, J., Doty, T., Gibson, B. & Heyer, W. D. Human BRCA2 protein promotes RAD51 filament formation on RPA-covered single-stranded DNA. *Nature structural & molecular biology* **17**, 1260-1262, doi:10.1038/nsmb.1904 (2010).
40 Subramanian, V., Fields, P. A. & Boyer, L. A. H2A.Z: a molecular rheostat for transcriptional control. *F1000prime reports* **7**, 01, doi:10.12703/P7-01 (2015).

41 Castano, J. *et al.* Expression of MLL-AF4 or AF4-MLL fusions does not impact the efficiency of DNA damage repair. *Oncotarget* **7**, 30440-30452, doi:10.18632/oncotarget.8938 (2016).
42 Cong, L. *et al.* Multiplex genome engineering using CRISPR/Cas systems. *Science* **339**, 819-823, doi:10.1126/science.1231143 (2013).
43 Zhang, Y., Werling, U. & Edelmann, W. SLiCE: a novel bacterial cell extract-based DNA cloning method. *Nucleic acids research* **40**, e55, doi:10.1093/nar/gkr1288 (2012).
44 Min, J., Feng, Q., Li, Z., Zhang, Y. & Xu, R. M. Structure of the catalytic domain of human DOT1L, a non-SET domain nucleosomal histone methyltransferase. *Cell* **112**, 711-723 (2003).
45 Hsu, P. D. *et al.* DNA targeting specificity of RNA-guided Cas9 nucleases. *Nature biotechnology* **31**, 827-832, doi:10.1038/nbt.2647 (2013).
46 Watson, J. V., Chambers, S. H. & Smith, P. J. A pragmatic approach to the analysis of DNA histograms with a definable G1 peak. *Cytometry* **8**, 1-8, doi:10.1002/cyto.990080101 (1987).